Journal of Power Sources 180 (2008) 46–55

Contents lists available at ScienceDirect

Journal of Power Sources

journal homepage: www.elsevier.com/locate/jpowsour

Hydrogen production through steam electrolysis: Model-based dynamic behaviour of a cathode-supported intermediate temperature solid oxide electrolysis cell

J. Udagawa [a,b], P. Aguiar [b], N.P. Brandon [b,*]

[a] Imperial Centre for Energy Policy and Technology, Centre for Environmental Policy, Imperial College London, London SW7 2AZ, UK
[b] Department of Earth Science and Engineering, Imperial College London, London SW7 2AZ, UK

ARTICLE INFO

Article history:
Received 7 January 2008
Received in revised form 5 February 2008
Accepted 15 February 2008
Available online 10 March 2008

Keywords:
Hydrogen production
Steam electrolyser
SOEC
Intermediate temperature
Planar
Dynamic model

ABSTRACT

Hydrogen production via steam electrolysis may involve less electrical energy consumption than conventional low temperature water electrolysis, reflecting the favourable thermodynamics and kinetics at elevated temperatures. In the present paper, a one-dimensional model of a cathode-supported planar intermediate temperature solid oxide electrolysis cell (SOEC) stack is employed to study the dynamic behaviour of such an electrolyser. The simulations found that step changes in the average current density cause the stack temperature to alter during both exothermic and endothermic operation. However, the temperature control, by the variation of the air flow through the stack, was predicted to be capable of returning the stack temperature to the initial value. Furthermore, the proposed control strategy is observed to reduce the interim temperature excursions between the initial and final steady states, suggesting that such a control strategy has a good potential to prevent the issues of cell component fracture, and transitions in stack operating mode, which are related to the temperature fluctuations during dynamic operation of an SOEC stack.

1. Introduction

Hydrogen is regarded as a leading future fuel candidate. It has the potential to address the environmental and energy security issues associated with fossil-derived hydrocarbon fuels. Among many hydrogen production methods, water electrolysis is a well-established technique, which is capable of producing carbon-free hydrogen if used in conjunction with renewable or nuclear energy. However, water electrolysis has not had a significant commercial penetration, mainly due to its high electricity consumption and associated high operating cost [1].

Steam electrolysis at elevated temperatures might offer a solution by consuming less electrical energy than is required at ambient conditions through a combination of favourable thermodynamics and kinetics [2]. Such a method of hydrogen production is performed using a solid oxide electrolysis cell (SOEC), which can be seen in simple terms as the reverse operation of a solid oxide fuel cell (SOFC), allowing the opportunity to apply recent developments in SOFCs to the field. An SOEC consists of a three-layer solid structure (composed of porous cathode, electrolyte and porous anode) and an interconnect plate. Steam is introduced at the cathode side of the solid structure where it is reduced to hydrogen, releasing oxide ions in the process. The oxide ions then migrate through the electrolyte to the anode where they combine to form oxygen molecules, releasing electrons. Although the use of proton conductors has also been investigated [3–5], yttria-stabilised zirconia (YSZ), which is an oxide ion conductor, is generally used for the electrolyte in SOECs. Typical materials for the cathode are nickel–YSZ cermets and those for the anode are perovskite oxides such as lanthanum manganite.

In SOFC technologies, there is increased interest in intermediate temperature SOFCs (IT-SOFCs), which typically operate between 823 and 1073 K, to allow for a wider range of materials, more cost effective SOFC fabrication methods [6] and increased durability. The reduction in operating temperature has also been seen in the field of SOECs, in the limited number of experimental projects reported over recent decades [7–9], where the temperature at which the cells are tested has decreased from 1273 to 1073 K. Initially SOECs were developed as tubular cell structures to avoid sealing problems, which is a major issue in segregating the produced H_2 and O_2 in planar cells, particularly over multiple thermal cycles [10]. Today, despite such sealing difficulties, the trend in cell design is to employ planar structures. A planar structure permits high packing density and significantly smaller hot volume in the system than that allowed by a tubular design [11], together with lower manu-

* Corresponding author. Tel.: +44 20 7594 5704; fax: +44 20 7594 7444.
E-mail address: n.brandon@imperial.ac.uk (N.P. Brandon).

0378-7753/$ – see front matter © 2008 Elsevier B.V. All rights reserved.
doi:10.1016/j.jpowsour.2008.02.026

Nomenclature

f_A^0	inlet flow rate of the anode streams (mol s^{-1})
F	Faraday's constant (C mol^{-1})
$\bar{j}$	average current density (A m^{-2})
L	cell length (m)
W	cell width (m)
$y_{O_2}^{mole}$	mole fraction of oxygen in the anode gas streams

Greek letters

ν_{O_2}	stoichiometric coefficient of oxygen
ψ	air ratio

facturing costs and shorter current paths, reducing the ohmic cell resistance [12]. A planar SOEC can be categorised as being either an electrolyte-supported or electrode-supported design. The former employs the electrolyte as the support structure and is suitable for high temperature operation in which the, often large, ohmic resistance associated with a thick electrolyte can be reduced. In an electrode-supported cell, on the other hand, one of the electrodes is the thickest part of the solid structure, supporting a thick film electrolyte, typically 10 μm or so in thickness. Such a design has been developed in order to minimise ohmic resistances in SOFCs operating at intermediate temperatures, and may also be applied to intermediate temperature SOECs (IT-SOECs).

To ensure a sufficient rate of H_2 production, an SOEC system must consist of several repeating cells assembled in stacks. An SOEC stack can function in either exothermic, endothermic or thermoneutral operating modes. During the operation of an SOEC system, heat is generated in the stack as the result of irreversible losses due to ohmic resistance and electrode overpotentials. These depend on operating conditions such as the stack temperature and average current density, as well as materials selection and cell and stack geometry. Fig. 1 shows examples of stack temperature distribution, produced by the one-dimensional model of a co-flow IT-SOEC stack described in a previous publication [13]. The modelled stack considers the cells with the flow of H_2 and H_2O on the cathode side, and of pure O_2 on the anode side of the solid structure. As the mixture of H_2 and H_2O travels along the stack (from left to right in the figure), H_2O is consumed by the reaction while H_2 and O_2 are produced. At the inlet to the cathode gas channels, 10 mol% H_2 is assumed sufficient in preventing the oxidation of the electrode material [7], while the inlet to the anode gas channels are sealed to allow the collection of pure O_2 from the outlet. An inlet temperature of 1023 K, an operating pressure of 0.1 MPa and a steam utilisation factor of 80% have been selected. For the steady-state simulation with an average current density of 7000 A m^{-2}, the heat generated via irreversible losses exceeds the thermal energy consumed by the endothermic electrolysis reaction. Such a condition is referred to as exothermic stack operation in which the temperature increases along the stack due to the heat accumulation, as indicated by the figure. Although exothermic operation provides the opportunity to bring the inlet gas streams to the operating temperature entirely through the recovery of the heat from the hotter outlet streams, such an operating mode is characterised by an increased electrical energy consumption by the stack. Conversely, for the simulation with an average current density of 5000 A m^{-2}, the heat generated via irreversible losses is predicted to be smaller than the thermal energy consumed by the reaction. Such a situation corresponds to endothermic stack operation in which the temperature decreases as the reaction proceeds along the stack. Although endothermic operation allows the stack to function with a lower electrical energy consumption, the rate of H_2 production per unit stack area is less than that arising from exothermic operation, evident from the lower average current density. Furthermore, during endothermic operation, it is not possible to bring the inlet streams to the operating temperature entirely by heat recovery from the outlet streams. The implication is that an external heat source is required to supply the thermal energy necessary to elevate the inlet stream temperature to the required level. Therefore, in the design of SOEC systems, there is a trade-off between the benefits of partially replacing electrical energy by less expensive thermal energy, against the extra costs involved in engineering the transfer of this thermal energy from external sources. Finally, thermoneutral stack operation occurs when the thermal energy consumed by the reaction is precisely matched by the heat generated via irreversible losses. During this mode of operation, although the outlet streams carry the same amount of thermal energy as the inlet streams, the energy losses associated with the heat recovery process mean that an external heat source and corresponding equipment costs would still be necessary, as in the case of endothermic operation. The electrical energy consumption of the stack during thermoneutral operation is, however, always greater than that during endothermic operation. Therefore, in general, thermoneutral operation is not recommended from an economic perspective [14].

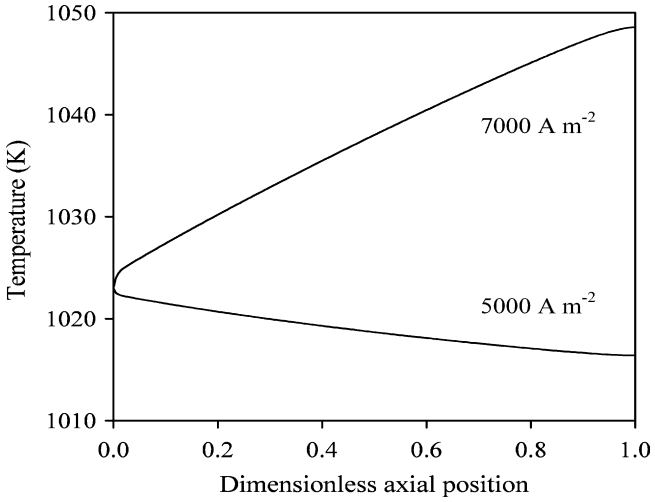

Fig. 1. Temperature distribution along the IT-SOEC stack described in a previous publication [13] for average current densities of 7000 and 5000 A m^{-2}, and an inlet temperature of 1023 K.

In a previous publication, a one-dimensional distributed dynamic model of a cathode-supported planar IT-SOEC stack has been presented [13]. The steady-state simulation of the model predicted an electricity consumption significantly less than that of low temperature stacks commercially available today. However, the dependence of the stack temperature distribution on the average current density, as can be seen in Fig. 1, calls for strict temperature control if such a stack is to be successfully built and used, especially in dynamic operation. Although SOEC systems are often considered for large-scale steady-state operation in which the input power source may be a nuclear reactor, temperature control becomes essential if the systems are to be used in dynamic operation with intermittent electrical power sources such as wind turbines or photovoltaic cells. To prevent the fracture of delicate stack components during dynamic operation, significant thermal excursions in the stack need to be avoided by the implementation of an effective control strategy. Such a control strategy could also aid to maintain a constant operating mode of the stack, which is an important constraint as the system requirements vary depending on whether the stack is employed in an exothermic, endothermic or thermoneutral mode. One possible solution to achieving the control requirements would be to modify the SOEC design such that one more degree of

freedom is available to control the stack temperature. As can be seen in [15], the temperature of an SOFC stack is often controlled by varying the air flow through the cells. Such a strategy may potentially be applied in the case of an SOEC stack where the introduction of air to the anode gas channels would, in addition to controlling the stack temperature, dilute the O_2 by-product. Although this would remove the possibility of generating extra revenues through the sale of pure O_2, it would also reduce the risk of high temperature corrosion, which might otherwise be caused by the exposure of metallic stack and balance of plant components to such a highly oxidising atmosphere at elevated temperatures [16]. The prospect of controlling the temperature of an SOEC stack through the change in the air flow rate has been discussed in [17]. The paper reported on the development of a dynamic model of a conceptual IT-SOEC stack with the air flow introduced through the cells and the simulated steady-state behaviour of such an electrolyser. The simulations found that the increase in the air flow rate provides enhanced cooling and heating for the stack during exothermic and endothermic operation, respectively. Such a change in the convective heat transfer between the cell components and air flow is expected to allow the control of the stack temperature. However, only a small dependence of the temperature on the air flow rate was observed for a stack driven at conditions near thermoneutral operation, indicating that this operating mode should be avoided from a control perspective.

A mathematical model is an important design tool for devices such as an SOEC, which are still in the development stage. It allows the prediction of the behaviour of the device under different process conditions and assists in the optimisation of its performance. In particular, such a model is essential in understanding the response of an electrolyser under steady electrical power input, such as those from the grid or nuclear energy, as well as under an intermittent renewable electrical power input. However, no studies on the dynamic behaviour of an SOEC can be found in the literature. The present paper focuses on the transient response of a conceptual IT-SOEC stack. A previously developed model of an IT-SOEC stack with air flow introduced through the cells [17] has been employed to predict the stack response during step changes in the average current density caused by the time dependent supply of electrical energy to or demand for hydrogen from the IT-SOEC. Simulations are performed with fixed and variable air flow rates to estimate the stack behaviour without and with the implementation of the temperature control, respectively. The potential of the control strategy to prevent such issues as fracture of the cell components, and transitions in stack operating mode, caused by the temperature fluctuations during dynamic operation of the stack is discussed.

2. IT-SOEC mathematical model

Although the number of modelling activities on electrolysis at elevated temperatures has increased over recent years [13,18–31], the mathematical modelling of SOEC stacks is still not an active research area. Today, only limited modelling studies attempting to describe SOEC stack behaviour can be found [13,26–31] and, to the authors' knowledge, the transient behaviour of an SOEC stack has not been the focus of any published work. Here, a previously developed one-dimensional dynamic model of a cathode-supported planar IT-SOEC stack [17] is used to report the simulated steady state and transient response of such an electrolyser. Key characteristics of the model are presented in this section. More detailed description is found in previous publications [13,17].

In an SOEC system, several repeating cells are assembled in stacks to support a sufficient rate of H_2 production. However, the models of such stacks are usually constructed for the smallest unit cell, which is assumed to describe the response of the whole stack, subject to the use of adequate boundary conditions. Here, the modelled unit cell is considered to be in the centre of a large stack such that end effects can be neglected. Although interconnects normally provide the gas flow channels, above and below the solid structure, the effect of individual passages is neglected. The pressure drop along the gas channels is also assumed to be negligible at the operating pressure of 0.1 MPa, and for the flow rates considered. For the purpose of developing the model, the unit cell is considered to be composed of four components, the cathode and anode gas streams, solid structure and interconnect. Fig. 2 shows the schematic view of such a unit cell. The model consists of an electrochemical model, mass balances for the cathode and anode streams, and energy balances for the cathode and anode streams, solid structure and interconnect. The properties of the gas streams, solid structure and interconnect are assumed to be uniform in order to achieve a more computationally tractable model. This simplification has been assessed in equivalent studies of IT-SOFC stacks in which the stack model employing uniform flow properties, determined at the inlet, and that employing variable flow properties have been compared [32]. The study showed that the simplification is justified provided the average current density is not high. Furthermore for the IT-SOEC stack model here the gas properties are averaged over the entire stack length, rather than using those determined at the inlet, to minimise the errors involved in using the uniform properties. Finally, ideal gas behaviour is assumed for the cathode and anode streams.

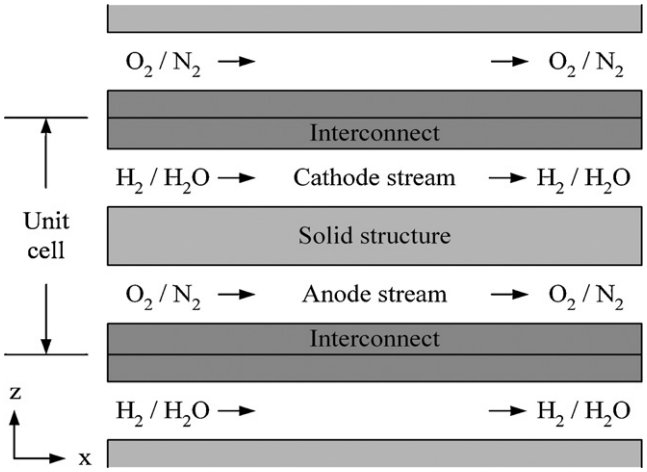

Fig. 2. Schematic view of a planar SOEC stack with the air flow through the anode channels.

The air ratio reflects the inlet flow rate of air in relation to the rate of reaction. It is here defined as the ratio between the moles of O_2 contained in the inlet air flow to that produced in the unit cell, per unit time. In spite of the slightly different physical definition, the mathematical description of the air ratio, provided in Eq. (1) for an SOEC, is equivalent to that of an SOFC [6]. Assuming that a minimum of 50 mol% N_2 in the anode streams at the stack outlet is required to limit the corrosion of metallic components, the lower bound for the air ratio can be selected to be as small as 0.4. The upper bound is assumed to be 14, namely the maximum air flow rate which can be supplied without incurring significant additional energy costs [15]

$$\psi = \frac{2Ff_A^0 y_{O_2}^{mole}(0)}{\bar{j}LW\nu_{O_2}}. \quad (1)$$

3. Simulation results and discussion

The system of partial differential and algebraic equations for the model of an IT-SOEC stack with air-fed anode channels is solved

Table 1
Important model input parameters and initial conditions for the exothermic and endothermic stacks

	Exothermic	Endothermic
Average current density (A m^{-2})	7000	5000
Air ratio	5.26	2.59
Inlet temperature of the cathode and anode streams (K)	923	1123

via the finite difference method using gPROMS Model Builder 3.0.3 [33]. The cathode and anode inlet compositions are assumed to be 10 mol% H_2/90 mol% H_2O and 21 mol% O_2/79 mol% N_2, respectively. The steam utilisation factor is selected to be 80%. The stack geometry and material properties can be found in a previous publication [13]. Section 3.1 defines the initial steady-state condition of the exothermic and endothermic stacks, presenting the cell potential and explaining the temperature distribution of individual cell components. The step changes in the average current density are imposed to such initial steady states to explore the transient response of the stack temperature and cell potential during the exothermic and endothermic operation in Sections 3.2 and 3.3, respectively. Such dynamic results are presented for the operation with the fixed and variable air ratios to evaluate the effectiveness of the temperature control strategy described in the previous sections.

3.1. Initial steady states

Before dynamic simulations of the IT-SOEC stack are performed, the initial steady-state conditions should be defined. Some important model input parameters and initial conditions, employed for the simulations of exothermic and endothermic stacks, to which step changes in the average current density are imposed, are shown in Table 1. The initial values of the air ratio have been selected to achieve the cathode stream outlet temperature of 1023 K, creating the temperature difference of 100 K between the inlet and outlet in both stacks. The temperature gradient of this scale is expected to result in a significant convective heat transfer between the cell components and air flow. From the previous work [17], the regulation of such a heat transfer, by the changes in the air ratio, is predicted to allow an effective control for the stack temperature. The rest of the model input parameters selected for the simulations could be found in a previous publication [13].

Figs. 3 and 4 present the contributions of the reversible potential and irreversible losses on the cell potential along the exothermic and endothermic stacks in the initial steady states, respectively.

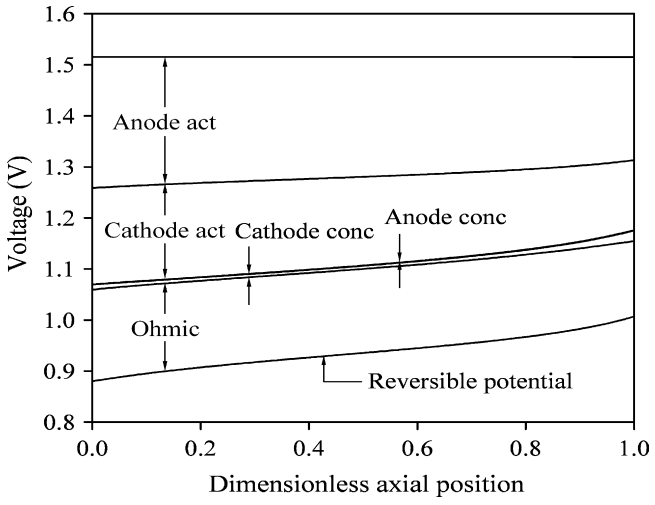

Fig. 3. Reversible potential and irreversible losses along the exothermic stack in the initial steady state.

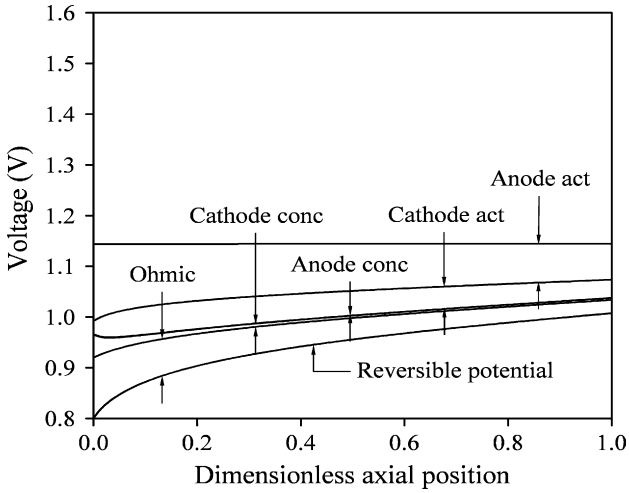

Fig. 4. Reversible potential and irreversible losses along the endothermic stack in the initial steady state.

In general, the activation overpotentials are observed to be the predominant source of irreversible losses while the concentration overpotentials are found negligible. The cell potential of around 1.52 V, observed in Fig. 3 for the exothermic stack, is significantly larger than the previously reported value [17] for the stack with an inlet temperature of 1023 K. Such an increase is attributed to the rise in both the reversible potential and irreversible losses caused by the reduced stack temperature. Conversely in Fig. 4, the inlet temperature of 1123 K for the endothermic stack results in the cell potential of around 1.14 V, significantly lower than that previously reported for the stack with an inlet temperature of 1023 K [17].

The local current density distributions along the exothermic and endothermic stacks in the initial steady states are shown in Fig. 5. While a positive local current density gradient is generally observed for the exothermic stack, the local current density decreases along the endothermic stack. Assuming a current efficiency of 100%, the local current density is directly proportional to the reaction rate. Therefore, the rise in the local current density towards the outlet of the exothermic stack indicates an increase in the reaction rate. Such an accelerated reaction, together with the increased H_2 partial pressure and the decreased H_2O partial pressure, is responsible for the rise in the cathode concentration overpotential near the stack outlet, shown in Fig. 3. For the endothermic stack, the large local

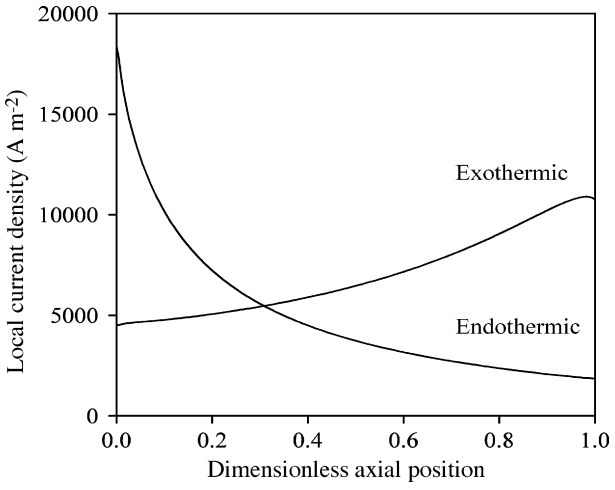

Fig. 5. Local current density along the exothermic and endothermic stacks in the initial steady states.

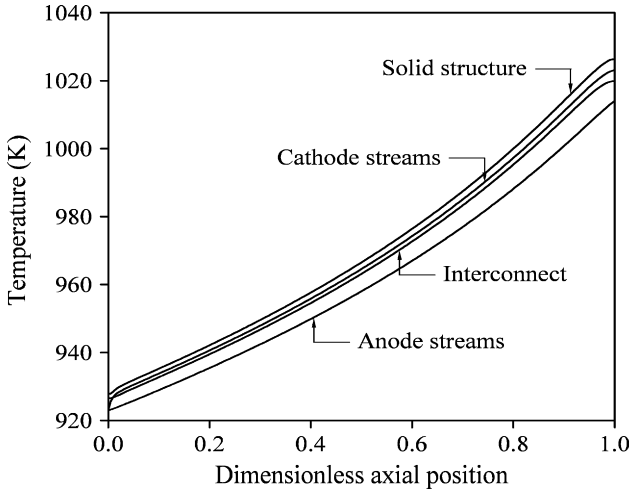

Fig. 6. Cathode and anode streams, solid structure and interconnect temperatures along the exothermic stack in the initial steady state.

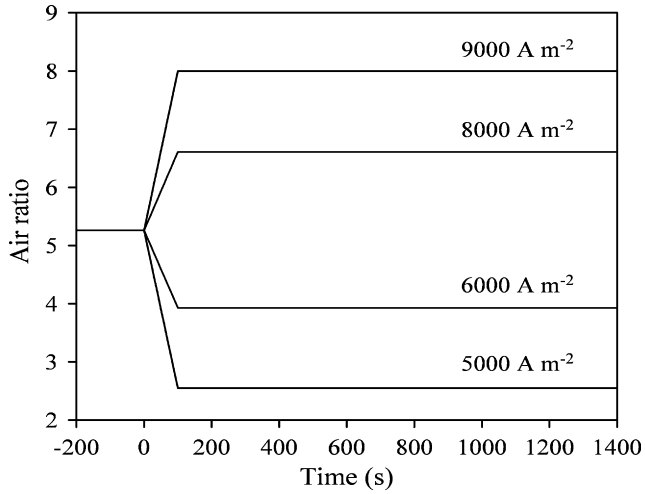

Fig. 8. Changes in the air ratio, which have been applied to the exothermic stack to imitate the action of an arbitrary controller during step changes in the average current density from 7000 to 5000, 6000, 8000 and 9000 A m^{-2}.

current density close to the inlet results in the increased cathode concentration overpotential at such a location, as observed in Fig. 4, in spite of the low H_2 and high H_2O partial pressures.

The temperature distributions along the exothermic and endothermic stacks in the initial steady states are presented in Figs. 6 and 7, respectively. In Fig. 6, the solid structure possesses the highest temperature at all locations along the stack as a result of the excess heat generated via irreversible losses while the anode streams have the lowest temperature due the presence of the air, providing cooling for the stack as it enters the anode channels at 923 K. The cathode stream temperature is found to rise rapidly near the stack inlet through the thermal interactions with the solid structure and interconnect. It is predicted to exceed the interconnect temperature within a short distance of the inlet. In Fig. 7, the temperature distribution of the endothermic stack shows an opposite trend to that of the exothermic stack. Here, the anode streams maintain the highest temperature along the stack owing to the heating provided by the air entering the stack at 1123 K. The thermal energy consumed by the reaction, which exceeds the heat generated via irreversible losses, results in the solid structure possessing the lowest temperature. The cathode stream temperature is observed to fall rapidly to the level below the interconnect temperature within a short distance of the inlet.

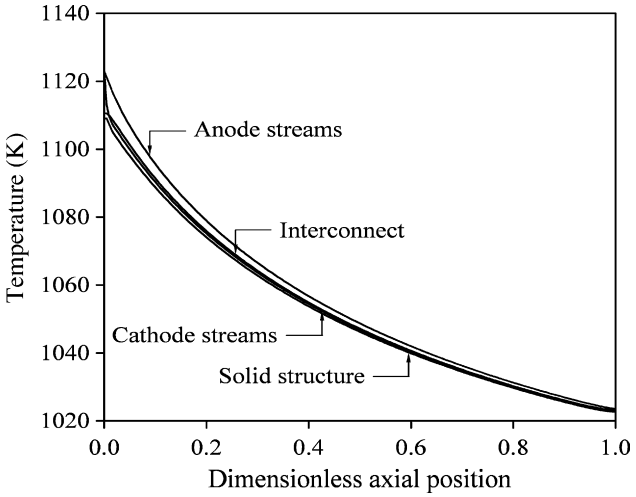

Fig. 7. Cathode and anode streams, solid structure and interconnect temperatures along the endothermic stack in the initial steady state.

3.2. Dynamic behaviour of IT-SOEC stack during exothermic operation

Figs. 8–12 present the transient response of the exothermic stack when step changes in the average current density from 7000 to 5000, 6000, 8000 and 9000 A m^{-2} are imposed on the initial steady state defined in Section 3.1. Such step changes have been selected to illustrate the stack behaviour under both the negative and positive disturbances in the input electrical power. The dynamic results are presented for the simulations in which the stack temperature is left uncontrolled as well as for those in which an attempt has been made to provide some temperature control. In the former, the air ratio has been maintained constant, while in the latter, it has been adjusted to imitate the action of an arbitrary controller. The transient response of the air ratio resulting from such a controller action is shown in Fig. 8. Here, the controller is assumed to progressively bring the air ratio to its final steady-state value over 100 s after the step changes in the average current density at the time of 0 s. The air ratio at the final steady state, which allows the

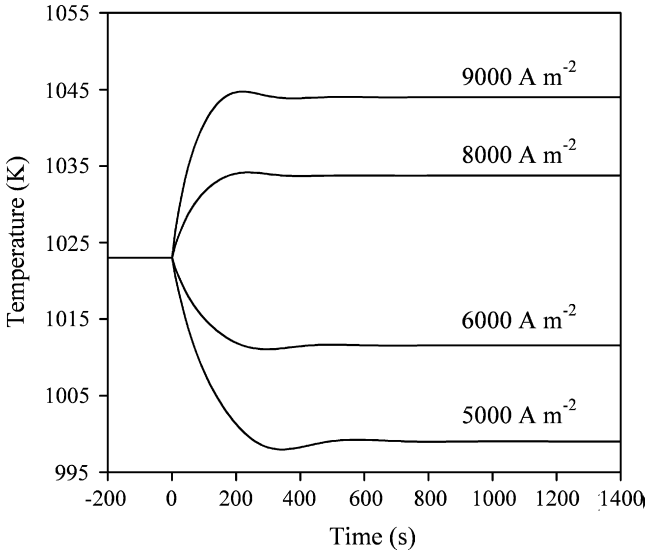

Fig. 9. Transient response of the cathode stream outlet temperature during step changes in the average current density from 7000 to 5000, 6000, 8000 and 9000 A m^{-2}, imposed on the exothermic stack without air ratio manipulation.

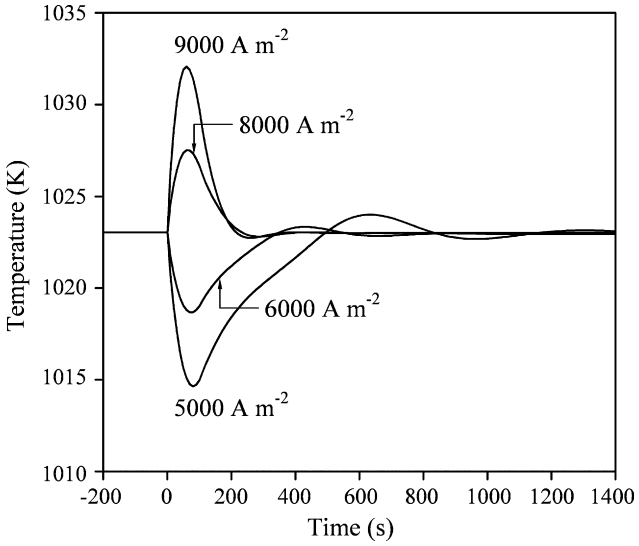

Fig. 10. Transient response of the cathode stream outlet temperature during step changes in the average current density from 7000 to 5000, 6000, 8000 and 9000 A m^{-2}, imposed on the exothermic stack with air ratio manipulation as illustrated in Fig. 8.

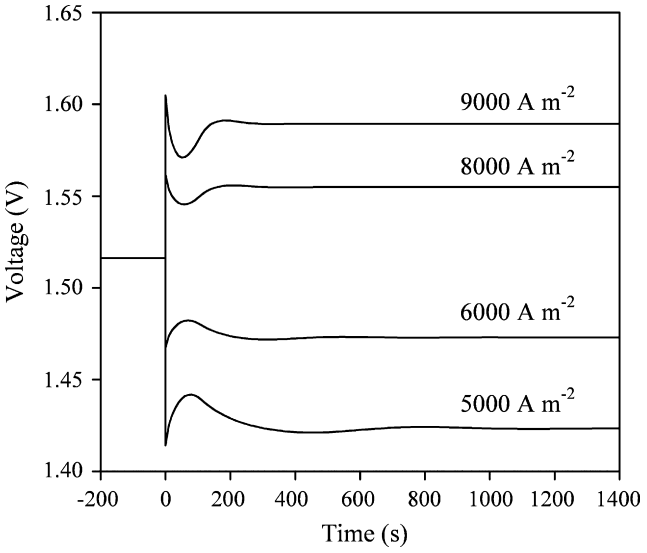

Fig. 12. Transient response of the cell potential during step changes in the average current density from 7000 to 5000, 6000, 8000 and 9000 A m^{-2}, imposed on the exothermic stack with air ratio manipulation as illustrated in Fig. 8.

cathode stream outlet temperature to return to its initial value, has been determined prior to the simulations. Note that the controller action is purposely selected to be rather slow here such that its effects on the stack temperature and cell potential would clearly appear in Figs. 10 and 12, respectively.

Fig. 9 shows the transient response of the cathode stream outlet temperature during step changes in the average current density imposed without air ratio manipulation. The stack temperature is monitored at the outlet as the greatest temperature transition is expected to occur at such a location. In the figure, a rapid fall in the outlet temperature is observed immediately after the negative step changes from 7000 to 5000 and 6000 A m^{-2}. As detailed previously [13], the decrease in the average current density causes a decrease in the heat generated via irreversible losses, reducing the stack temperature. Conversely, a rapid rise in the outlet temperature follows the positive step changes from 7000 to 8000 and 9000 A m^{-2} due to the increase in the heat generated via irreversible losses. The minimum outlet temperature of around 998 K is reached following the step decrease in the average current density to 5000 A m^{-2} while the maximum outlet temperature of around 1045 K is reached shortly after the step increase to 9000 A m^{-2}. These values correspond to the temperature fall and rise, from the initial stack outlet temperature, of 25 and 22 K, respectively.

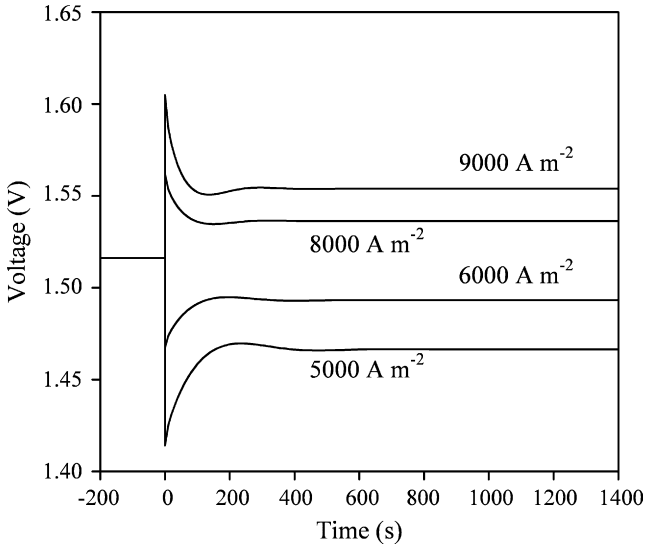

Fig. 11. Transient response of the cell potential during step changes in the average current density from 7000 to 5000, 6000, 8000 and 9000 A m^{-2}, imposed on the exothermic stack without air ratio manipulation.

The transient response of the cathode stream outlet temperature during step changes in the average current density imposed with air ratio manipulation is presented in Fig. 10. Similarly to Fig. 9, Fig. 10 shows the rapid fall and rise in the outlet temperature immediately follow the negative and positive step changes, respectively. Here, the outlet temperature is, however, eventually returned to its initial value by the manipulation of the air ratio. After a negative step change, the decrease in the air ratio results in decreased convective cooling of the stack, causing the stack temperature to rise back up to the initial value. Conversely, after a positive step change, the increase in air ratio results in increased convective cooling of the stack, allowing the stack temperature to be brought back down to the initial value. During such temperature transitions, the minimum outlet temperature of around 1015 K and the maximum outlet temperature of around 1032 K are reached following the step decrease to 5000 A m^{-2} and step increase to 9000 A m^{-2}, respectively. These correspond to the temperature fall of 8 K and rise of 9 K from the initial steady-state value, indicating that the control strategy is not only able to return the outlet temperature to its initial value but also reduces the interim temperature excursions. The outlet temperature in Fig. 10 is characterised by oscillations which are clearly more pronounced for the negative step changes than for the positive step changes. Although such a difference in the dynamic stack response cannot be explained at this stage, it is subject to future investigation.

Fig. 11 shows the transient response of the cell potential during step changes in the average current density imposed without air ratio manipulation. Here, the difference in the response time between the cell potential and stack temperature results in an undershoot and overshoot in voltage observed for the negative and positive step changes, respectively. During a negative step change, the cell potential is instantaneously decreased due to an immediate fall in irreversible losses. The stack temperature, on the other hand, is reduced over a greater time interval as shown in Fig. 9. Such a reduction in the stack temperature causes the irreversible losses to progressively rise, increasing the cell potential until the final

steady state is reached. Conversely, during a positive step change, the increase in the average current density triggers an immediate rise in the cell potential which then progressively decreases to its final steady-state value as the stack temperature is elevated. The undershoot following the negative step change to 5000 A m^{-2} causes the minimum cell potential of around 1.41 V while the overshoot after the step change to 9000 A m^{-2} results in the maximum cell potential of around 1.60 V. Such minimum and maximum cell potentials correspond to a decrease of 7.24%, and an increase of 5.26%, from the initial steady-state value.

The transient response of the cell potential during step changes in the average current density imposed with air ratio manipulation is illustrated in Fig. 12. Although the cell potential is again characterised by an undershoot or overshoot, its final steady-state value differs from that of the simulations with the fixed air ratio, presented in Fig. 11. The final cell potential here is associated with the stack temperature which has been returned to the initial value, as well as the new O_2 partial pressure in the anode streams corresponding to the air ratio at the final steady state. The cell potential at the final steady state in Fig. 12 is found to be lower following the negative step changes and higher after the positive step changes than those in Fig. 11. This suggests that although the air ratio manipulation successfully provides the temperature control for the exothermic stack, it also results in an increased transition in the cell potential between the initial and final steady states. For the negative step change to 5000 A m^{-2}, the cell potential at the final steady state is around 1.42 V, which corresponds to a decrease of 6.58% with respect to the initial steady-state value. For the positive step change to 9000 A m^{-2}, the final cell potential is around 1.59 V, corresponding to an increase of 4.61%. Such small transitions are not expected to cause problems during the operation of an SOEC stack.

This section presented the simulated dynamic behaviour of the IT-SOEC stack operated under exothermic conditions. Although the results indicate that the step changes in the average current density cause the outlet temperature to alter rapidly, manipulation of the air ratio is capable of returning the temperature to the initial value. Such a control strategy is observed to also reduce the interim temperature excursions between the initial and final steady states. As previously mentioned, the controller action is purposely selected to be rather slow in the simulations presented here. In practice, an actual controller with more rapid response would be capable of reducing the interim temperature excursions further, and allowing the final steady state to be reached more promptly, than illustrated in the simulated results. Nevertheless, the transient response of the outlet temperature displayed in Fig. 10 still suggests that the proposed control strategy has a good potential in preventing the issues related to the temperature fluctuations during dynamic operation of the exothermic stack.

3.3. *Dynamic behaviour of IT-SOEC stack during endothermic operation*

Figs. 13, 14 and 16–18 present the transient response of the endothermic stack when step changes in the average current density from 5000 to 3000, 4000, 6000 and 7000 A m^{-2} are imposed on the initial steady state defined in Section 3.1. The dynamic results are presented for simulations in which the air ratio has been fixed as well as for those in which the air ratio has been adjusted to provide some temperature control. Fig. 13 shows the transient response of the air ratio resulting from such a controller action. Similarly to the exothermic stack in Fig. 8, the air ratio is assumed to be progressively brought to its final steady-state value in 100 s after the step changes in the average current density. The air ratio at the final steady state, which allows the cathode stream outlet temperature to return to its initial value, has again been determined

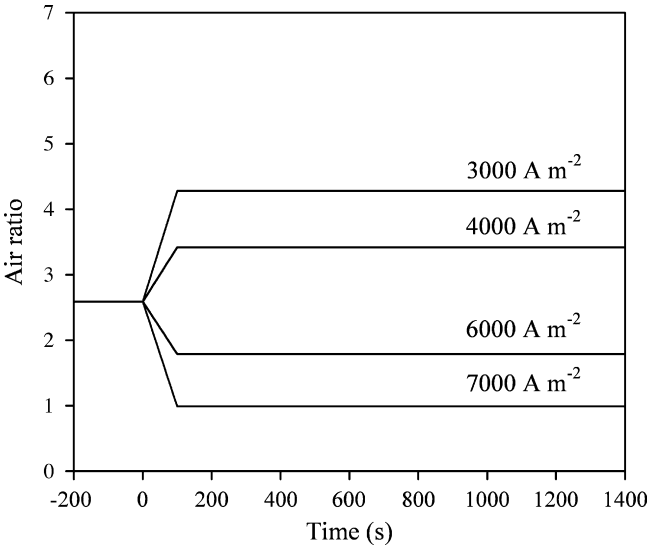

Fig. 13. Changes in the air ratio, which have been applied to the endothermic stack to imitate the action of an arbitrary controller during step changes in the average current density from 5000 to 3000, 4000, 6000 and 7000 A m^{-2}.

prior to the simulations. Note that a rather slow controller action is again selected, allowing its effects on the stack temperature and cell potential to clearly be observed in Figs. 16 and 18, respectively. Also note that the transient response of the air ratio, presented for the endothermic stack, in Fig. 13 possesses an opposite trend to that of the exothermic stack in Fig. 8. During endothermic operation, the increase in the air ratio results in increased convective heating to the stack. Therefore, the decrease in the heat generated via irreversible losses, following the negative step changes in the average current density from 5000 to 3000 and 4000 A m^{-2}, can be compensated by the increased air ratio. After the positive step changes from 5000 to 6000 and 7000 A m^{-2}, on the other hand, the increase in the heat generated via irreversible losses is offset by the decreased air ratio.

Fig. 14 shows the transient response of the cathode stream outlet temperature during step changes in the average current density imposed without air ratio manipulation. Similarly to the exothermic stack, the fall and rise in the average current density cause the

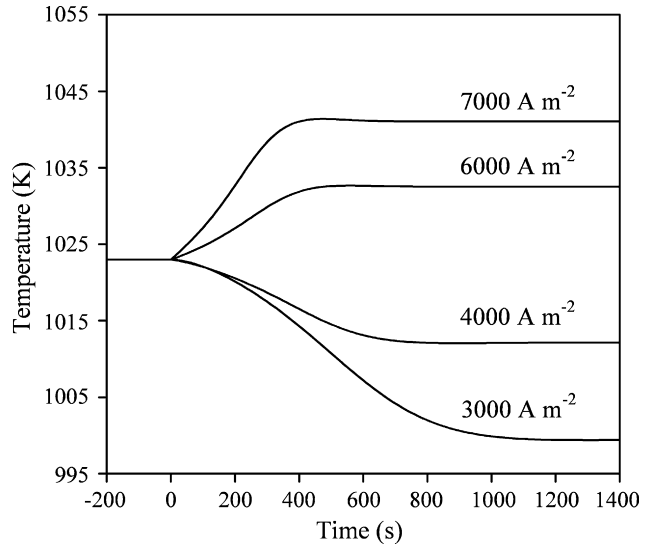

Fig. 14. Transient response of the cathode stream outlet temperature during step changes in the average current density from 5000 to 3000, 4000, 6000 and 7000 A m^{-2}, imposed on the endothermic stack without air ratio manipulation.

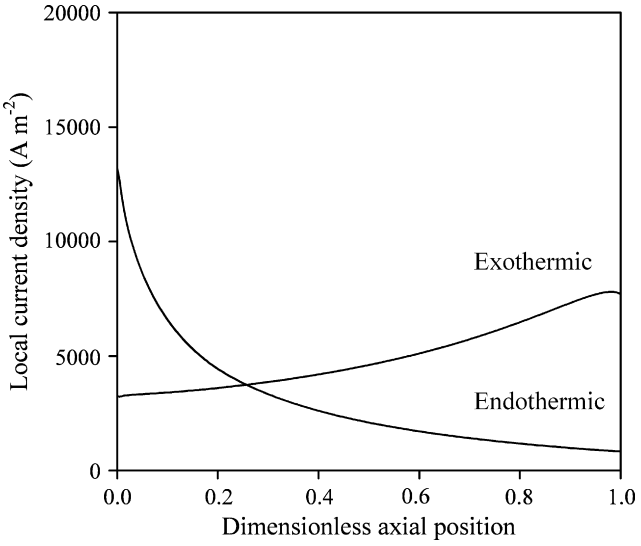

Fig. 15. Local current density along the exothermic and endothermic stacks immediately after the negative step changes in the average current density from 7000 to 5000 A m^{-2} and from 5000 to 3000 A m^{-2}, respectively.

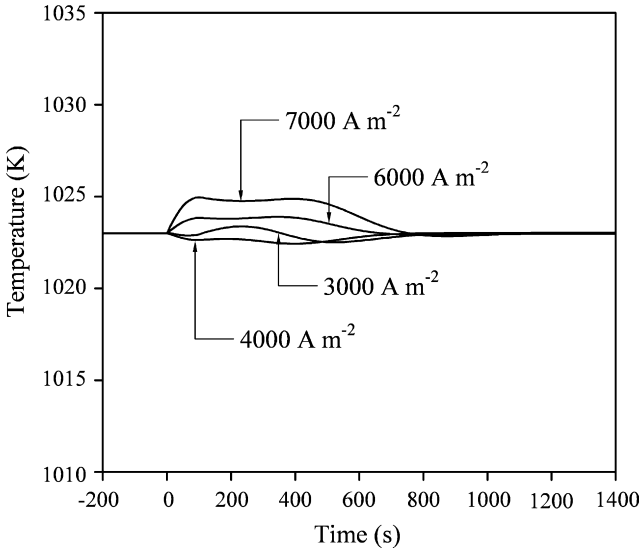

Fig. 16. Transient response of the cathode stream outlet temperature during step changes in the average current density from 5000 to 3000, 4000, 6000 and 7000 A m^{-2}, imposed on the endothermic stack with air ratio manipulation as illustrated in Fig. 13.

temperature of the endothermic stack to decrease and increase, respectively. However, the change in the outlet temperature of the endothermic stack occurs at slower rates than those of the exothermic stack shown in Fig. 9. This is due to the difference between the exothermic and endothermic stacks in how the local current density distribution evolves during dynamic operation. As an example, the local current density distribution of the exothermic stack immediately after the negative step change in the average current density from 7000 to 5000 A m^{-2}, and that of the endothermic stack immediately after the negative step change from 5000 to 3000 A m^{-2}, are illustrated in Fig. 15. From the comparison with the initial steady states in Fig. 5, it is apparent that the step changes trigger the greatest decrease in the local current density near the outlet of the exothermic stack and near the inlet of the endothermic stack. For the exothermic stack, the significant fall in the local current density and the corresponding reduction in irreversible losses at the stack outlet result in the rapidly decreasing outlet temperature displayed in Fig. 9. For the endothermic stack, on the other hand, the significant fall in the local current density and the corresponding reduction in irreversible losses at the stack inlet promote the heat transfer towards the inlet, gradually decreasing the outlet temperature as shown in Fig. 14. Together with the heat conduction within the solid structure, such a heat transfer along the stack takes place via the thermal energy carried in the gas streams, as they travel along the channels, and via convection between the streams and solid structure. Note that for constant steam utilisation and air ratio, negative and positive step changes cause a decrease and increase in the stream flow rates, respectively. For the conditions presented in Fig. 14, the final flow rates for both the cathode and anode streams following the step changes to 3000 A m^{-2} are less than half of those after the step changes to 7000 A m^{-2}. Here, the slower heat transfer associated with the smaller stream flow rates is reflected in the figure as the outlet temperature, which requires longer time to reach the final steady state following the negative step changes than after the positive step changes.

The transient response of the cathode stream outlet temperature during step changes in the average current density imposed with air ratio manipulation is presented in Fig. 16. The figure shows that the air ratio manipulation successfully returns the outlet temperature to the initial value with maximum interim temperature excursion of only around 2 K, observed following the positive step change to 7000 A m^{-2}. The temperature excursions are maintained within such a low level due to the delayed response of the outlet temperature, following the step changes. This allows a considerable change in the air ratio to take place before a significant departure in the outlet temperature occurs from the initial value. Furthermore, between the initial and final steady states, the outlet temperature is observed to be generally higher following the negative step change to 3000 A m^{-2} than after the negative step change to 4000 A m^{-2}. This is inconsistent with the trend displayed in Fig. 14 in which, without the temperature control, a greater reduction in the outlet temperature is predicted following the step change to 3000 A m^{-2}. As can be seen in Fig. 13, however, the controller is assumed to increase the air ratio at a faster rate following the step change to 3000 A m^{-2} than after the step change to 4000 A m^{-2}. Therefore, when the temperature control is implemented, the correspondingly faster rise in the convective heating maintains the higher outlet temperature following the step change to 3000 A m^{-2}. The outlet temperature is brought back to the initial value within 800 s after all step changes.

Fig. 17 shows the transient response of the cell potential during step changes in the average current density imposed without air ratio manipulation. Similarly to the exothermic stack in Fig. 11, undershoots and overshoots are associated with the negative and positive step changes, respectively. Here, the undershoot following the negative step change to 3000 A m^{-2} causes the minimum cell potential of around 1.07 V while the overshoot after the step change to 7000 A m^{-2} results in the maximum cell potential of around 1.21 V. Such minimum and maximum cell potentials both correspond to a decrease and increase of 6.14%, from the initial steady-state value.

The transient response of the cell potential during step changes in the average current density imposed with air ratio manipulation is illustrated in Fig. 18. Similarly to the exothermic stack, the cell potential at the final steady state here is lower following the negative step changes and higher after the positive step changes than those of the stack without air ratio manipulation, presented in Fig. 17. For the negative step change to 3000 A m^{-2}, the cell potential at the final steady state is around 1.08 V, which corresponds to a decrease of 5.26% with respect to the initial steady-state value. For the positive step change to 7000 A m^{-2}, the final cell potential is around 1.21 V, corresponding to an increase of 6.14%. As previously mentioned for the exothermic stack, such small transitions

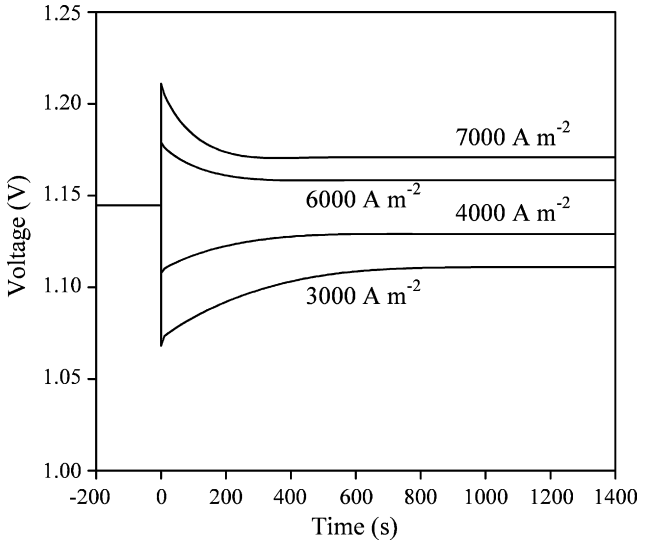

Fig. 17. Transient response of the cell potential during step changes in the average current density from 5000 to 3000, 4000, 6000 and 7000 A m^{-2}, imposed on the endothermic stack without air ratio manipulation.

are not expected to cause problems during the operation of an SOEC stack.

This section presented the simulated dynamic behaviour of the IT-SOEC stack operated under endothermic conditions. Similarly to the exothermic stack, the outlet temperature of the endothermic stack is altered following the step changes in the average current density. Such a temperature transition is, however, estimated to occur at slower rates than in the exothermic stack, allowing a considerable action by the controller to take place before a significant departure in the outlet temperature from the initial value occurs. As the result, the controller is predicted to return the outlet temperature to the initial value with only small interim temperature excursions, suggesting that the proposed control strategy should be capable of preventing the issues related to the temperature fluctuations during dynamic operation of the endothermic stack also.

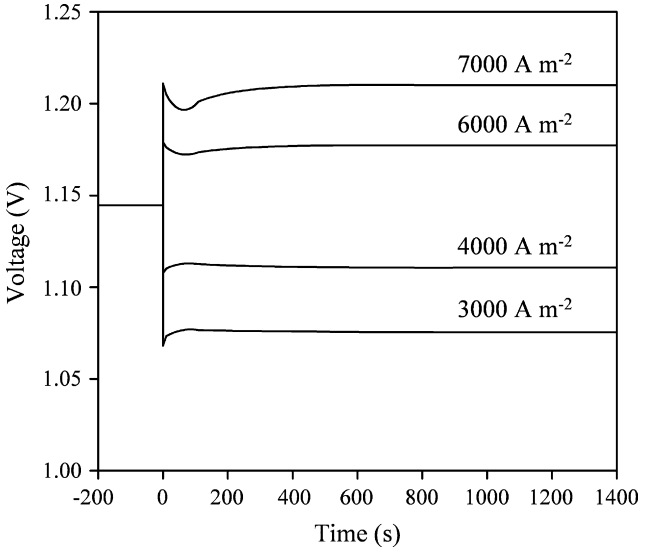

Fig. 18. Transient response of the cell potential during step changes in the average current density from 5000 to 3000, 4000, 6000 and 7000 A m^{-2}, imposed on the endothermic stack with air ratio manipulation as illustrated in Fig. 13.

4. Conclusions

A one-dimensional distributed dynamic model of a cathode-supported planar IT-SOEC stack with the air flow introduced through the cells [17] has been employed to study the dynamic behaviour of such an SOEC and the prospect for stack temperature control through variation of the air flow rate. The step changes in the average current density were imposed to the stacks operated under exothermic and endothermic conditions, replicating the situation in which the changes in the supply of input electrical energy or demand for hydrogen are experienced. Such simulations have been performed both without and with the manipulation of the air ratio, imitating the action of an arbitrary controller. The simulated results suggest that although the stack temperature is altered by the step changes in the average current density, the proposed control strategy is capable of returning the outlet temperature of both exothermic and endothermic stacks to the initial value. Furthermore, the interim temperature excursions between the initial and final steady states are observed to be reduced by the action of the controller. Dynamic simulations also indicated that undershoot or overshoot appear in the cell potential when the step changes in the average current density are imposed. The control of stack temperature was observed to have an effect of increasing the difference between the cell potential at the initial steady state and that at the final steady state. The cell potential transitions are, however, predicted to be small such that they are not expected to cause problems during the operation of an SOEC stack.

References

[1] D.L. Stojic, M.P. Marceta, S.P. Sovilj, S.S. Miljanic, J. Power Sources 118 (2003) 315–319.
[2] S. Dutta, Int. J. Hydrogen Energy 15 (1990) 379–386.
[3] T. Kobayashi, K. Abe, Y. Ukyo, H. Matsumoto, Solid State Ionics 138 (2001) 243–251.
[4] T. Schober, Solid State Ionics 139 (2001) 95–104.
[5] H. Matsumoto, M. Okubo, S. Hamajima, K. Katahira, H. Iwahara, Solid State Ionics 152/153 (2002) 715–720.
[6] P. Aguiar, C.S. Adjiman, N.P. Brandon, J. Power Sources 138 (2004) 120–136.
[7] J.S. Herring, J.E. O'Brien, C.M. Stoots, G.L. Hawkes, J.J. Hartvigsen, M. Shahnam, Int. J. Hydrogen Energy 32 (2007) 440–450.
[8] W. Donitz, E. Erdle, Int. J. Hydrogen Energy 10 (1985) 291–295.
[9] R. Hino, K. Haga, H. Aita, K. Sekita, Nucl. Eng. Des. 233 (2004) 363–375.
[10] W. Doenitz, R. Schmidberger, Int. J. Hydrogen Energy 7 (1982) 321–330.
[11] J.S. Herring, P. Lessing, J.E. O'Brien, C. Stoots, J. Hartvigsen, S. Elangovan, Proceedings of the 2nd Information Exchange Meeting on Nuclear Production of Hydrogen, 2003, pp. 183–200.
[12] J. Larminie, A. Dicks, Fuel Cell Systems Explained, 2nd ed., Wiley, 2003.
[13] J. Udagawa, P. Aguiar, N.P. Brandon, J. Power Sources 166 (2007) 127–136.
[14] K.H. Quandt, R. Streicher, Int. J. Hydrogen Energy 11 (1986) 309–315.
[15] P. Aguiar, C.S. Adjiman, N.P. Brandon, J. Power Sources 147 (2005) 136–147.
[16] G.Y. Lai, High-Temperature Corrosion of Engineering Alloys, ASM International, 1990.
[17] J. Udagawa, P. Aguiar, N.P. Brandon, J. Power Sources, in press.
[18] B. Yildiz, M.S. Kazimi, Int. J. Hydrogen Energy 31 (2006) 77–92.
[19] F. Werkoff, J. Sigurvinsson, C. Mansilla, P. Lovera, Proceedings of the 16th World Hydrogen Energy Conference, 2006, CD-ROM.
[20] J. Sigurvinsson, C. Mansilla, P. Lovera, F. Werkoff, Int. J. Hydrogen Energy 32 (2007) 1174–1182.
[21] J. Sigurvinsson, C. Mansilla, B. Arnason, A. Bontemps, A. Marechal, T.I. Sigfusson, F. Werkoff, Energy Convers. Manage. 47 (2006) 3543–3551.
[22] Y. Shin, W. Park, J. Chang, J. Park, Int. J. Hydrogen Energy 32 (2007) 1486–1491.
[23] M. Saxe, P. Alvfors, Energy 32 (2007) 42–50.
[24] J.W. Park, Y.J. Lee, Proceedings of the 2006 International Congress on Advances in Nuclear Power Plants, 2006, CD-ROM.
[25] C. Mansilla, J. Sigurvinsson, A. Bontemps, A. Marechal, F. Werkoff, Energy 32 (2007) 423–430.
[26] M. Ni, M.K.H. Leung, D.Y.C. Leung, Electrochim. Acta 52 (2007) 6707–6718.
[27] M. Ni, M.K.H. Leung, D.Y.C. Leung, Int. J. Hydrogen Energy 32 (2007) 2305–2313.

[28] P. Lovera, F. Blein, J. Vulliet, Proceedings of the 16th World Hydrogen Energy Conference, 2006, CD-ROM.
[29] E. Hoashi, T. Ogawa, K. Matsunaga, K. Nakada, S. Fujiwara, S. Kasai, Proceedings of the 2006 International Congress on Advances in Nuclear Power Plants, 2006, CD-ROM.
[30] G.L. Hawkes, J.E. O'Brien, C.M. Stoots, J.S. Herring, M. Shahnam, Nucl. Technol. 158 (2007) 132–144.
[31] G. Hawkes, J. O'Brien, C. Stoots, J. Herring, R. Jones, Proceedings of the 2006 Fuel Cell Seminar, 2006, CD-ROM.
[32] P. Iora, P. Aguiar, C.S. Adjiman, N.P. Brandon, Chem. Eng. Sci. 60 (2005) 2963–2975.
[33] Process Systems Enterprise Ltd., gPROMS Introductory User Guide (2002).